11th International Workshop on Ship and Marine Hydrodynamics
Hamburg, Germany, September 22-25, 2019

Numerical Study on Steady Wave Drift Forces of an Obliquely Moving Ship

W. Zhang[1]*, O. el Moctar[2]

[1]China University of Petroleum (East China), School of Petroleum Engineering, 66 West Changjiang Road, Qingdao, 266580, China PR
[2]University of Duisburg-Essen, Institute of Ship Technology and Ocean Engineering, 69 Bismarckstr., Duisburg, 47057, Germany

*Corresponding author, weizhang@upc.edu.cn

ABSTRACT

This paper considers numerical computation of the steady wave drift forces acting on an obliquely moving ship. The traditional forward speed seakeeping problem was extended to consider the ship with a drift angle. A computer code was developed based on a time domain Rankine panel method. Once the velocity potential around the hull was determined, the first order wave induced motions were calculated and then the second order wave drift forces were evaluated using a near field method. Based on the developed code, the longitudinal and transverse steady wave drift force, as well as the steady yaw moment were computed for a container ship in head and beam waves. The effects of the drift angle on the steady wave drift forces were included and discussed. The numerical results were compared with the published experimental measurements, which shows fairly good agreement.

1 INTRODUCTION

In recent years, ship maneuverability in waves have been increasingly investigated. Several related works (eg. Skejic and Faltinsen[1]; Yasukawa and Nakayama[2]; Seo and Kim[3]) demonstrated that the wave drift forces have remarkable influence on the ships' maneuvering performance. An accurate evaluation of wave drift forces is essential to correctly predict the ship maneuvering motions in waves, such as turning circles and zigzag maneuvers.

In fact, prediction of the wave drift forces acting on the ship have been one of the most interesting topics in marine hydrodynamics. Most of the related studies focused on predicting the steady longitudinal wave drift force, which is also referred to as the wave added resistance (Raw). Nowadays, it has become possible to theoretically predict the added resistance of ships using either potential flow theory or CFD approach with acceptable accuracy for practical purposes. For example, Joncquez[4] used a time domain Rankine panel method to obtain the linearized potential and computed the wave added resistance using the near field and far field method. Also, using a time domain Rankine panel method, Kim and Kim[5] calculated wave added resistance of several kinds of ships and discussed the added resistance in irregular waves. Söding et al.[6] computed the wave added resistance via a frequency domain Rankine panel method that accounts for the dynamic squat of the ship and the effects of the nonlinear steady flow caused by the ship's forward speed. El Moctar et al.[7] , Sigmund and el Moctar[8] presented results of wave added resistance by solving the Reynolds-averaged Navier-Stokes (RANS) equations.

Compared to the large amount of works on the wave added resistance, few studies have been made on the steady transverse drift force and the related yaw moment. Most of the contributions in this field are based on the experimental measurement. Naito et al.[9] measured the wave-induced steady forces on a motion constrained Esso-Osaka tanker advancing in oblique waves and compared the measured data with their numerical results. Ueno et al.[10] measured the steady wave forces and moment on a VLCC model maneuvering in short waves. Sprenger et al.[11] presented the model test data of the added resistance and drift forces at zero and moderate forward speed, for the KVLCC2 tanker and the DTC container ship.

Recently, there were also a few numerical studies on steady transverse drift force and yaw moment. Wicaksono and Kashiwagi[12] employed the enhanced unified theory and a new strip method to evaluated the Kochin function, then computed the steady forces and yaw moment of a ship advancing in oblique waves. Yasukawa et al.[13] computed the wave-induced steady forces by using a zero-speed 3D panel method and a strip theory-based Kochin-function method. They also compared their numerical results with the experimental measurements.

The above mentioned works provided practical methods for predicting the steady drift force and yaw moment on the ships. However, almost all the existing methods considered only the ship straightly advancing in waves. From the point of predicting the ship maneuvering in waves, it is still questionable whether these theoretical methods could be directly employed, because the ship will always have a drift angle during the maneuvering. By carrying out physical model test, Yasukawa and Adnan[14] found that the drift forces acting on an obliquely moving ship could differ from the forces on a straightly moving one. Therefore, including the effect of the drift angle in the numerical method seem to be necessary for a more precise prediction of the wave drift forces and moment on the ship in maneuvering condition

In this study, we conducted numerical computation of the steady wave drift forces of an obliquely moving ships. We extended the boundary value problem (BVP) of the classical seakeeping problem to describe the flow field around the ship with a drift angle. The extended BVP was solved via a time domain Rankine panel method and the wave drift forces were computed using a near-field method. We carried numerical computations for the S-175 containership advancing in head and beam waves. The steady longitudinal, transverse drift forces and the steady yaw moment (hereinafter referred to as the steady surge force, the steady sway force and the steady yaw moment, respectively), were computed firstly for the ship in straightly advancing condition to validate the developed code. Then we computed the steady drift forces and the steady yaw moment for the ship with a drift angle. The computed drift forces and yaw moment were compared against published experimental measurements (Yasukawa and Adnan[14]).

2 MATHEMATICAL BACKGROUND

2.1 Boundary Value Problem

Two right-handed coordinate systems are adopted in the present study as shown in Fig. 1. The first one *o-xyz* is a horizontally moving mean-body fixed coordinate system. The positive *x*-coordinate points towards the bow and the positive *z*-coordinate points upward. The *xy* plane always coincides with the calm water level, and the origin of the coordinate system is located amidships. The translatory displacements in the *x*-, *y*- and *z*- directions are ξ_1 (surge), ξ_2 (sway)and ξ_3 (heave), and the angular displacements about the *x*-, *y*- and *z*-axes are ξ_4 (roll), ξ_5 (pitch) and ξ_6 (yaw) respectively. The second one *O-XYZ* is a global frame fixed in space, which is used to define the encountering angle χ of the incident waves. The positive drift angle is defined as the ship speed rotates clockwise from the *x*-axis.

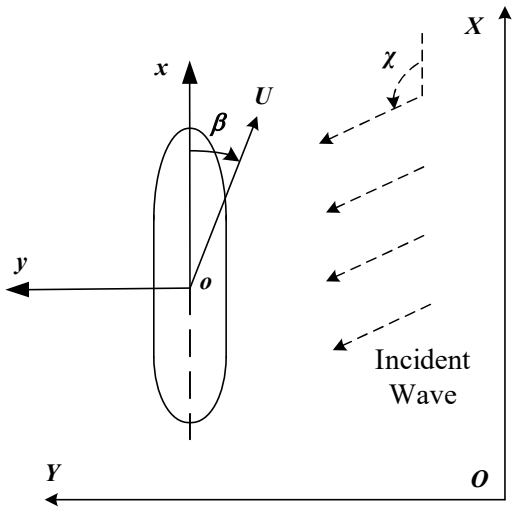

Figure 1: The coordinate systems

Let us consider a ship travelling in regular waves with a constant speed U and a drift angle β. Under the assumption that the fluid is inviscid and incompressible, and the flow is irrotational, a velocity potential $\Psi(\bar{x},t)$ can be introduced, which satisfies the following boundary value problem (BVP):

$$\nabla^2\Psi = 0 \quad \text{in fluid domain} \tag{1}$$

$$[\frac{\partial}{\partial t} - (\vec{U} - \nabla\Psi)\cdot\nabla]\zeta_T = \frac{\partial\Psi}{\partial z} \quad \text{on} \quad z=\zeta_T(x,y,t) \tag{2}$$

$$[\frac{\partial}{\partial t} - (\vec{U} - \nabla\Psi)\cdot\nabla]\Psi = -g\zeta_T + \frac{1}{2}\nabla\Psi\cdot\nabla\Psi \quad \text{on} \quad z=\zeta_T(x,y,t) \tag{3}$$

$$\frac{\partial\Psi(\bar{x},t)}{\partial n} = \vec{U}\cdot\vec{n} + \frac{\partial\vec{\delta}}{\partial t}\cdot\vec{n} \quad \text{on body surface} \tag{4}$$

where $\vec{U} = (u,v,0) = (U\cos\beta, -U\sin\beta, 0)$, $\bar{x} = (x,y,z)$, $\vec{n}$ is the inward unit normal vector on the hull surface (out of fluid); $\vec{\delta}$ is the oscillatory displacement of the hull surface due to the wave induced motion, $\zeta_T(x,y,t)$ is the wave elevation, g is the gravitational acceleration and t denotes time.

We linearized the boundary conditions Eqs.(2-4) using the double-body linearization scheme. To this end, the velocity potential and the free surface elevation are decomposed as follows:

$$\Psi(\bar{x},t) = -ux - vy + \Phi(\bar{x}) + \varphi_I(\bar{x},t) + \varphi(\bar{x},t) + \phi(\bar{x},t) \tag{5}$$

$$\zeta_T(x,y,t) = \zeta_I(x,y,t) + \zeta(x,y,t) \tag{6}$$

where $\Phi(\bar{x})$ is the double body potential, $\varphi_I(\bar{x},t)$ represents the incident wave potential, $\zeta_I(x,y,t)$ is the incident wave elevation. $\varphi(\bar{x},t)$ and $\phi(\bar{x},t)$ denote the disturbed wave potential and local potential, respectively. $\zeta(x,y,t)$ is the wave elevation related to the disturbed wave potential $\varphi(\bar{x},t)$. The double body potential is assumed to be the main component with its order of $O(1)$, while other parts are assumed smaller than $\Phi(\bar{x})$ by one order of magnitude and they have the order of $O(\varepsilon)$. Here ε is of the order of magnitude of A/L where A and L are the wave amplitude and the length of the ship. It is assumed that $\varepsilon \ll 1$.

The incident wave potential is defined as:

$$\varphi_I(\bar{x},t) = A\frac{g}{\omega_0}e^{kz}\sin[k(x\cos\chi + y\sin\chi) - \omega_e t] \tag{7}$$

where A is the amplitude of the incident wave, ω_0 is the frequency of the incident wave, k is the wave number, $k = \omega_0^2/g$ for deep water, ω_e is the encounter frequency defined as:

$$\omega_e = |\omega_0 - k(u\cos\chi + v\sin\chi)| \tag{8}$$

The double-body potential Φ is determined by the following boundary conditions:

$$\begin{cases} \dfrac{\partial\Phi}{\partial n} = \vec{U}\cdot\vec{n}, & \text{on } \bar{S} \\ \dfrac{\partial\Phi}{\partial z} = 0, & \text{on z=0} \end{cases} \tag{9}$$

where $\bar{S}$ is the mean wetted hull surface.

The local potential $\phi(\bar{x},t)$ is employed to model the instantaneous response of the fluid to the ship motions. The linearized BVP for $\phi(\bar{x},t)$ read as:

$$\begin{cases} \dfrac{\partial\phi}{\partial n} = \sum_{j=1}^{6}(\dfrac{\partial\xi_j}{\partial t}n_j + \xi_j m_j) & \text{on } \bar{S} \\ \phi = 0 & \text{on z=0} \end{cases} \tag{10}$$

where n_j is defined as the generalized normal vector

$$
\begin{aligned}
&(n_1, n_2, n_3) = \vec{n} \\
&(n_4, n_5, n_6) = \vec{x} \times \vec{n}
\end{aligned} \tag{11}
$$

and m_j is the so-called *m*-terms (Newman[15]), which can be evaluated using the basic flow:

$$
\begin{aligned}
&(m_1, m_2, m_3) = (\vec{n} \cdot \nabla)(\vec{U} - \nabla\Phi) \\
&(m_4, m_5, m_6) = (\vec{n} \cdot \nabla)\left[\vec{x} \times (\vec{U} - \nabla\Phi)\right]
\end{aligned} \tag{12}
$$

In practice, the *m*-terms are calculated using the numerical scheme proposed by Wu[16].

The local potential $\phi(\vec{x}, t)$ can be further decomposed according the modes of the ship motions, each mode is defined as

$$
\phi_i = N_i(\vec{x})\dot{\xi}_i(t) + M_i(\vec{x})\xi_i(t) \quad i = 1, 2, \ldots, 6 \tag{13}
$$

where $\dot{\xi}_i(t)$ and $\xi_i(t)$ denote the velocity and displacement of the mode *i*, respectively. The canonical potential $N_i(\vec{x})$ and $M_i(\vec{x})$ satisfy the following boundary conditions:

$$
\begin{cases}
\dfrac{\partial N_i}{\partial n} = n_i, \dfrac{\partial M_i}{\partial n} = m_i \quad \text{on } \bar{S} \\
N_i = 0, M_i = 0 \quad \text{on z=0}
\end{cases} \tag{14}
$$

The linearized boundary value problems for wave potential $\varphi(\vec{x}, t)$ read as follows:

$$
\begin{cases}
\nabla^2\varphi = 0 \\
\varphi = \dfrac{\partial\varphi}{\partial t} = 0 \quad \text{at} \quad t = 0 \\
[\dfrac{\partial}{\partial t} - (\vec{U} - \nabla\Phi) \cdot \nabla]\zeta = \dfrac{\partial^2\Phi}{\partial z^2}(\zeta + \zeta_I) + \dfrac{\partial\varphi}{\partial z} + \dfrac{\partial\phi}{\partial z} - \nabla\Phi \cdot \nabla\zeta_I \quad \text{on} \quad \text{z=0} \\
[\dfrac{\partial}{\partial t} - (\vec{U} - \nabla\Phi) \cdot \nabla]\varphi = -g\zeta - \nabla\Phi \cdot \nabla\varphi_I \quad \text{on} \quad \text{z=0} \\
\dfrac{\partial\varphi}{\partial n} = -\dfrac{\partial\varphi_I}{\partial n} \quad \text{on } \bar{S} \\
\text{Radiation condition}
\end{cases} \tag{15}
$$

2.2 First Order Wave Forces and Wave-Induced Ship Motions

According to Newton's law, the 6 degrees of freedom (6DOF) equations of wave-induced ship motion read as follows

$$
\sum_{j=1}^{6}[m_{ij}\ddot{\xi}_j(t) + c_{ij}\xi_j(t)] = F_i(\ddot{\vec{\xi}}, \dot{\vec{\xi}}, \vec{\xi}, t) \quad i = 1, 2, \ldots, 6 \tag{16}
$$

where m_{ij} denotes the element of the inertial matrix for the hull, c_{ij} is hydrostatic restoring coefficients. $\{F_i\} = (F_x, F_y, F_z, M_x, M_y, M_z)$ denotes the generalized first order hydrodynamic forces.

The first order hydrodynamic pressure is divided and computed as follows:

$$
p = p_l + p_m + p_I = -\rho[\frac{\partial}{\partial t} - (\vec{U} - \nabla\Phi) \cdot \nabla](\phi + \varphi + \varphi_I) \tag{17}
$$

where the subscripts *l*, *m, I* denote the pressure related the local potential, memory potential and incident potential, respectively.

The first order hydrodynamic forces can be determined by:

$$
F_i = F_i^L + F_i^W = \iint_{\bar{S}} p_l n_i ds + \iint_{\bar{S}} (p_m + p_I) n_i ds \quad i = 1, 2, \ldots, 6 \tag{18}
$$

By introducing the following notations

$$\begin{cases} a_{ij}^L = \rho \iint_{\bar{S}} (N_j) n_i ds \\ b_{ij}^L = \rho \iint_{\bar{S}} [-(\bar{U} - \nabla\Phi) N_j + M_j] n_i ds \\ c_{ij}^L = \rho \iint_{\bar{S}} [-(\bar{U} - \nabla\Phi) M_j] n_i ds \end{cases} \tag{19}$$

we can turn the equations of motion into the following form:

$$\sum_{j=1}^{6} [(m_{ij} + a_{ij}^L)\ddot{\xi}_j + b_{ij}^L \dot{\xi}_j + (c_{ij} + c_{ij}^L)\xi_j] = F_i^W \quad i = 1, 2, \ldots, 6 \tag{20}$$

Form Eq.(20) we can see the hydrodynamic forces which are related to the ship motions are moved to the left hand side of the equations. Since the canonical potential $N_k(\bar{x})$ and $M_k(\bar{x})$ are time independent, they could be solved and stored before computing the ship motions. The time domain simulation of the ship motions consists of the iteratively solving the BVP of the memory potential Eq.(15) and the equations of motions Eq.(20).

2.3 Formulation of Second Order Wave Forces and Moments

The generalized second-order hydrodynamic force, $\bar{F}^{(2)} = (F_x^{(2)}, F_y^{(2)}, F_z^{(2)}, M_x^{(2)}, M_y^{(2)}, M_z^{(2)})$, is evaluated using the following near-field pressure integration formula:

$$\begin{aligned} \frac{1}{\rho}\bar{F}^{(2)} = & \frac{1}{2}\int_{WL} g(\zeta - \xi_z)^2 \bar{n}^{(0)} dl - \int_{WL} \left\{ \nabla[-\bar{U}\cdot\nabla\Phi + \frac{1}{2}\nabla\Phi\cdot\nabla\Phi]\cdot\bar{\xi} \right\} (\zeta - \xi_z)\bar{n}^{(0)} dl \\ & - \int_{WL} [-\bar{U}\cdot\nabla\Phi + \frac{1}{2}\nabla\Phi\cdot\nabla\Phi](\zeta - \xi_z)\cdot\bar{n}^{(1)} dl \\ & - \frac{1}{2}\iint_{\bar{S}} (\nabla\varphi_P\cdot\nabla\varphi_P)\bar{n}^{(0)} ds - \iint_{\bar{S}} [H\bar{x}\cdot\nabla(-\bar{U}\cdot\nabla\Phi + \frac{1}{2}\nabla\Phi\cdot\nabla\Phi + gz)]\bar{n}^{(0)} ds \\ & - \iint_{\bar{S}} \left\{ \frac{\partial\varphi_P}{\partial t} - (\bar{U} - \nabla\Phi)\cdot\nabla\varphi_P + g\xi_z + \nabla[-\bar{U}\cdot\nabla\Phi + \frac{1}{2}\nabla\Phi\cdot\nabla\Phi]\cdot(\bar{\xi}_T + \bar{\xi}_R\times\bar{x}) \right\} \bar{n}^{(1)} ds \\ & - \iint_{\bar{S}} \left\{ \nabla[\frac{\partial\varphi_P}{\partial t} - (\bar{U} - \nabla\Phi)\cdot\nabla\varphi_P]\cdot(\bar{\xi}_T + \bar{\xi}_R\times\bar{x}) \right\} \bar{n}^{(0)} ds - \iint_{\bar{S}} (-\bar{U}\cdot\nabla\Phi + \frac{1}{2}\nabla\Phi\cdot\nabla\Phi + gz)\bar{n}^{(2)} ds \end{aligned} \tag{21}$$

where $\bar{\xi}_T = (\xi_1, \xi_2, \xi_3)$, $\bar{\xi}_R = (\xi_4, \xi_5, \xi_6)$, $\xi_z = \xi_3 + \xi_4 y - \xi_5 x$. $\bar{n}^{(1)} = \bar{\xi}_R \times \bar{n}$ and $\bar{n}^{(2)} = H\bar{n}$ denote the first- and second-order components of the normal vector on the hull surface, respectively. *H* stands for a matrix of the transformation, which is the defined as:

$$H = \frac{1}{2}\begin{bmatrix} -(\xi_5^2 + \xi_6^2) & 0 & 0 \\ 2\xi_4\xi_5 & -(\xi_4^2 + \xi_6^2) & 0 \\ 2\xi_4\xi_6 & 2\xi_5\xi_6 & -(\xi_4^2 + \xi_5^2) \end{bmatrix} \tag{22}$$

The mean values of the first, second and sixth components of $\bar{F}^{(2)}$ is the steady surge force, the steady sway force and the steady yaw moment acting on the hull. Details of deriving Eqs.(21) and (22) can be found in Joncquez[4].

3 NUMERICAL IMPLEMENTATION

3.1 Time domain Rankine Panel Method

The disturbed wave potential $\varphi(\bar{x}, t)$ is computed using a time domain Rankine Panel method. By applying the Green's identity and choosing the Rankine source as the basic singularity, we get the boundary integral equation for $\varphi(\bar{x}, t)$ reads as:

$$2\pi\varphi(\vec{x})+\iint_{\bar{F}\cup\bar{S}}\varphi\frac{\partial G(\vec{x}',\vec{x})}{\partial n'}d\vec{x}'-\iint_{\bar{F}\cup\bar{S}}\frac{\partial\varphi}{\partial n'}G(\vec{x}',\vec{x})d\vec{x}'=0 \tag{23}$$

where $\bar{S}$ is the mean wetted hull surface and $\bar{F}$ is the undisturbed free surface. G is the Rankine source:

$$G(\vec{x}',\vec{x})=1/\left|\vec{x}'-\vec{x}\right| \tag{24}$$

The fluid domain boundaries ($\bar{F}\cup\bar{S}$) are discretized by a number of plane quadrilateral panels. Following the approach of Kring[17], we assume the velocity potential φ as well as the free surface elevation ζ and the normal flux on the free surface φ_z are slowly varying on the panels. The variation is approximated by using the quadratic B-Spline basis function

$$\begin{cases}\zeta(\xi,\eta,t)\simeq\sum\limits_{j=-\infty}^{\infty}\zeta_j(t)B_j(\xi,\eta)=\sum\limits_{j=-\infty}^{\infty}\zeta_j(t)[b_j(\xi)\cdot b_j(\eta)]\\ \varphi_z(\xi,\eta,t)\simeq\sum\limits_{j=-\infty}^{\infty}(\varphi_z)_j(t)B_j(\xi,\eta)=\sum\limits_{j=-\infty}^{\infty}(\varphi_z)_j(t)[b_j(\xi)\cdot b_j(\eta)]\\ \varphi(\xi,\eta,t)\simeq\sum\limits_{j=-\infty}^{\infty}\varphi_j(t)B_j(\xi,\eta)=\sum\limits_{j=-\infty}^{\infty}\varphi_j(t)[b_j(\xi)\cdot b_j(\eta)]\end{cases} \tag{25}$$

where (ξ,η) is the local coordinate of each panel. The coefficients $\zeta_j(t)$, $(\varphi_z)_j(t)$ and $\varphi_j(t)$ are considered as the spatially discrete unknowns.

The one dimensional quadratic B-Spline basis function is defined as

$$b_j^{(2)}(\xi)=\begin{cases}\dfrac{1}{2h_\xi^2}(\xi+\dfrac{3h_\xi}{2})^2\ , & -3h_\xi/2<\xi<-h_\xi/2\\ \dfrac{1}{h_\xi^2}(-\xi^2+\dfrac{3h_\xi^2}{4})\ , & -h_\xi/2<\xi<h_\xi/2\\ \dfrac{1}{2h_\xi^2}(-\xi+\dfrac{3h_\xi}{2})^2\ , & h_\xi/2<\xi<3h_\xi/2\end{cases} \tag{26}$$

where h_ξ is the panel dimension.

Since the basis function can be differentiated analytically up to twice, the gradients of ζ and φ can be simply written as

$$\begin{cases}\nabla\zeta(\vec{x},t)\simeq\sum\limits_{j=-\infty}^{\infty}\zeta_j(t)\nabla B_j(\vec{x})\\ \nabla\varphi(\vec{x},t)\simeq\sum\limits_{j=-\infty}^{\infty}\varphi_j(t)\nabla B_j(\vec{x})\end{cases} \tag{27}$$

By substituting Eq.(27) into the linearized free surface conditions and approximating the temporal derivative by using explicit and implicit Euler schemes in kinematic and dynamic free surface conditions respectively, we can get the discreted boundary conditions on free surface, which are shown in Eq. (28) and (29). Note that summation for the multiply occurring indices need to be adopted in these equations.

$$\frac{\zeta_j^{(n+1)}-\zeta_j^{(n)}}{\Delta t}B_{ij}-\zeta_j^{(n)}(\bar{U}-\nabla\Phi)\cdot\nabla B_{ij}=(\zeta_j^{(n)}B_{ij}+\zeta_I)\Phi_{zz}+(\varphi_z)_j^{(n)}B_{ij}-\nabla\Phi\cdot\nabla\zeta_I \tag{28}$$

$$\frac{\varphi_j^{(n+1)}-\varphi_j^{(n)}}{\Delta t}B_{ij}-\varphi_j^{(n+1)}(\bar{U}-\nabla\Phi)\cdot\nabla B_{ij}=-\zeta_j^{(n+1)}gB_{ij}-\nabla\Phi\cdot\nabla\varphi_I \tag{29}$$

The Eqs.(23), (28) and (29) are solved by the collocation approach with the geometric center of the panels to be the collocation point. At time $t=t_{n+1}$, the kinematic condition (28) uses the solution of vertical flux of the free surface at $t=t_n$ (i.e. $(\varphi_z)_j^{(n)}$) to update the wave elevation. The dynamic condition (29) uses the wave elevation just obtained (i.e. $\zeta_j^{(n+1)}$) to update the potential. The integral equation (23) is then solved to determine the vertical flux on free surface and the potential on hull surface. More details about the Rankine panel method have been provided in Zhang and el Moctar[18].

3.2 Roll damping and Soft spring system

We determine the ship roll damping according to the ITTC's 'Numerical Estimation of Roll Damping Procedure'[19]. The total roll damping is divided into the wave (B_W), frictional(B_F), eddy (B_E) and lift (B_L) components:

$$B_{44} = B_W + B_F + B_E + B_L \tag{30}$$

The wave damping component has been already incorporated in the present potential computation. The other contributions are considered to be the extra rolling damping, which need to be added into the equation of ship roll motion. A non-dimensionalized roll damping coefficient $\hat{B}_{44EXT}$ is defined as

$$\hat{B}_{44EXT} = \hat{B}_F + \hat{B}_E + \hat{B}_L = \frac{B_F + B_E + B_L}{\rho \nabla B^2} \sqrt{\frac{B}{2g}} \tag{31}$$

The component of $\hat{B}_{44EXT}$ is evaluated according to the empirical formulae proposed by ITTC[19].

As there are no restoring forces for wave-induced horizontal motions (i.e., surge, sway and yaw), some artificial mechanism needs to be introduced to restrict the drift motion of the ship. A popular method is employing a soft spring system. This is also the case in the present study. To this end, we changed three elements on the diagonal of the hydrostatic matrix in Eq. (23) as

$$c_{ii} = S_i \cdot (\frac{\omega_e}{2})^2 \cdot (m_{ii}), \quad i = 1,2,6 \tag{32}$$

where the coefficients S_i is used to adjust the strength of the spring.

4 RESULT AND DISCUSSION

Based on the above, we developed a computer code and performed numerical computations for the S-175 container ship. The principal particulars of S-175 container ship are listed in Table 1.

Table 1: Main particulars of subject ship

Description [units]	Symbols	S-175 Containership	
		Full scale	Model scale(1:50)
Length bet. perp. [m]	L	175.0	3.5
Breadth [m]	B	25.4	0.508
Draft [m]	D	9.5	0.19
Displacement [m^3]	∇	24742	0.1936
Block coefficient	C_b	0.57	0.57
Vertical center of gravity [m]	KG	9.25	0.2075
x-coordinate of COG [m]	X_{CG}	-	-0.509
Metacentric height	GM	1.25	0.025
Radius of gyration in roll [m]	k_{xx}	-	0.15242
Radius of gyration in pitch [m]	k_{yy}	-	0.0952
Radius of gyration in yaw [m]	k_{zz}	-	0.0952

We carried out the numerical simulation with a ship model of the scale ratio 1/50. The extra roll damping coefficient is $\hat{B}_{44EXT} = 0.002764$; while the strength parameters of the soft spring system are chosen as

$$S_1 = 5.46 / (\frac{\omega_e}{2})^2, \; S_2 = 6.48 / (\frac{\omega_e}{2})^2, \; S_6 = 14.5 / (\frac{\omega_e}{2})^2$$

These values are evaluated according to the strength of the spring system used in the physical model test. More details of the physical model test could be found in Yasukawa and Adnan[14].

Two wave encountering angles, namely χ=180° (head wave) and χ=-90° (beam wave, the wave propagates for port side to starboard) was investigated. First, we computed 6DOF RAOs, as well as the steady drift forces and steady yaw moment for the ship straightly advancing in head and beam waves, to validate the proposed numerical method. Then we conducted numerical simulation of the ship moving in beam waves with a drift angle. Three drift angels are tested in the computations, including β=-10°, -5°, 5°. A

fixed ship forward speed, $Fn = U/\sqrt{gL} = 0.15$, is considered in all the computations. The respective normalized coefficients of the steady drift forces and moment are defined as follows:

$$C_x = \frac{-\bar{F}_x^{(2)}}{\rho g A^2 (B^2/L)}, \quad C_y = \frac{-\bar{F}_y^{(2)}}{\rho g A^2 (B^2/L)}, \quad C_N = \frac{-\bar{M}_z^{(2)}}{\rho g A^2 B^2} \tag{33}$$

where L is ship length between perpendiculars, and B is ship breadth at the waterline. Note here the computed steady yaw moment was initially about the origin of the *o-xyz* coordinate system. To be consistent with the model test results, we transferred our computed steady yaw moment to the moment about the center of gravity(COG) before comparing them to the experimentally measurements of Yasukawa and Adnan[14].

Numerical computations started from computing the motion RAOs and the added resistance for the S-175 container ship straightly advancing in head waves. Figure 2 illustrates the predicted wave-induced surge, heave and pitch RAOs, while Figure 3 the predicted wave added resistance. The present results are compared with the experimentally measured data of Yasukawa and Adnan[14]. As seen, although there are some discrepancies, the overall agreements between the present results and the experimental data are satisfactory. The peak value of the predicted heave motions is higher than the experimentally measured values. This is probably due to the neglect of the nonlinear effect. Similar result was also reported by Huang[20].

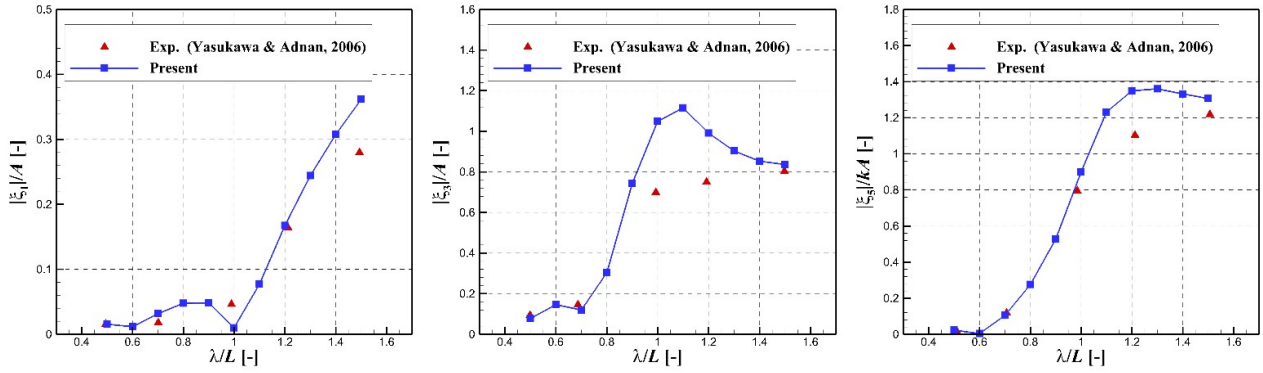

Figure 2: Motion RAOs for the S-175 container ship straightly advancing in regular head waves

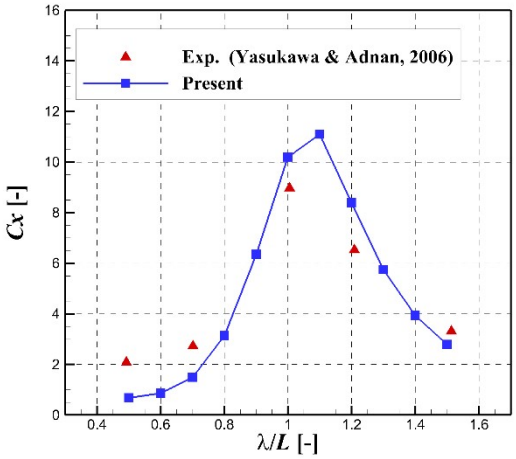

Figure 3: Added resistance for the S-175 container ship straightly advancing in regular head waves

Figure 4 illustrates the comparison between the computed and experimentally measured 6DOF RAOs for the S-175 container ship straightly advancing in beam waves. As seen, the predicted results captured the variations of the wave induced motions against the incident wave length. The predicted amplitudes of surge and sway are a little smaller than the experiment in shorter wave length range, while the predicted amplitudes of heave roll and pitch are slightly smaller than the measured ones in longer wave range. Nevertheless, the overall agreement between the predicted and measured 6 DOF RAO is generally acceptable.

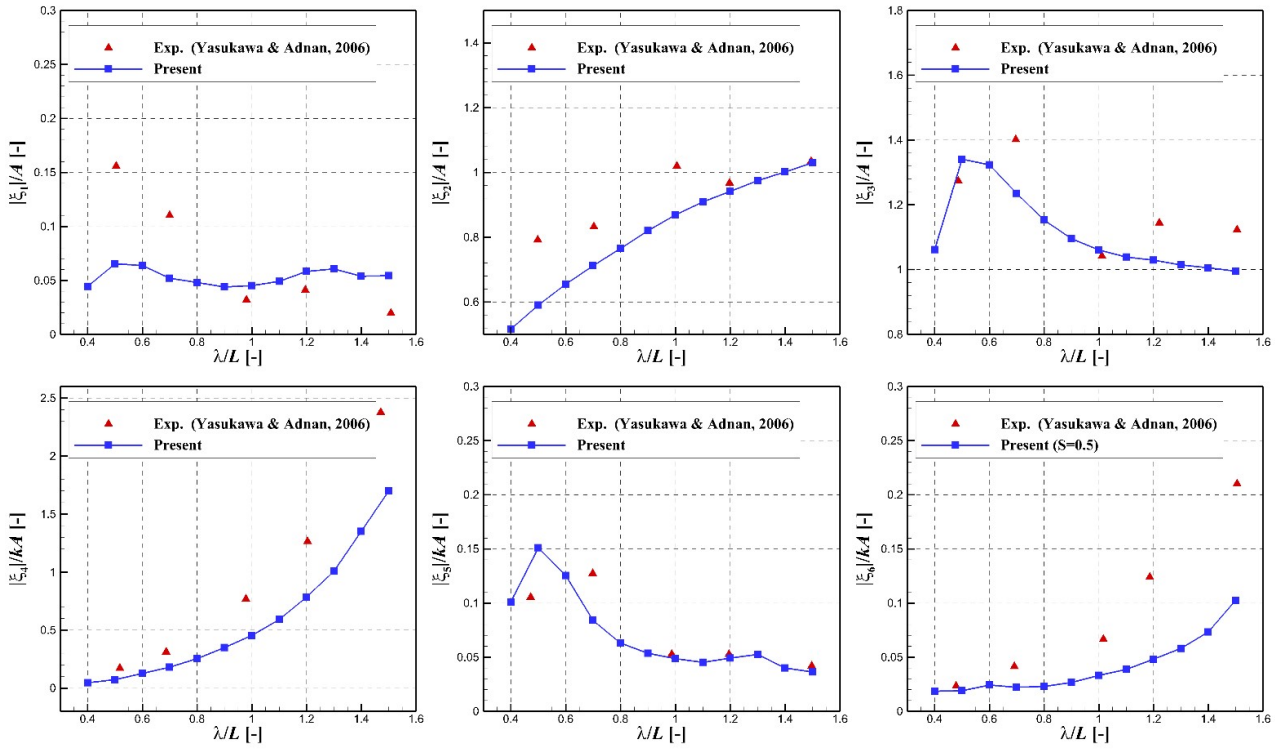

Figure 4: Motion RAOs for the S-175 container ship straightly advancing in regular beam waves

Figure 5 shows the steady surge force, the steady sway force and the steady yaw moment for S-175 container ship straightly advancing in beam waves. Again the numerical results are compared with the experimental measurements provided by Yasukawa and Adnan[14].

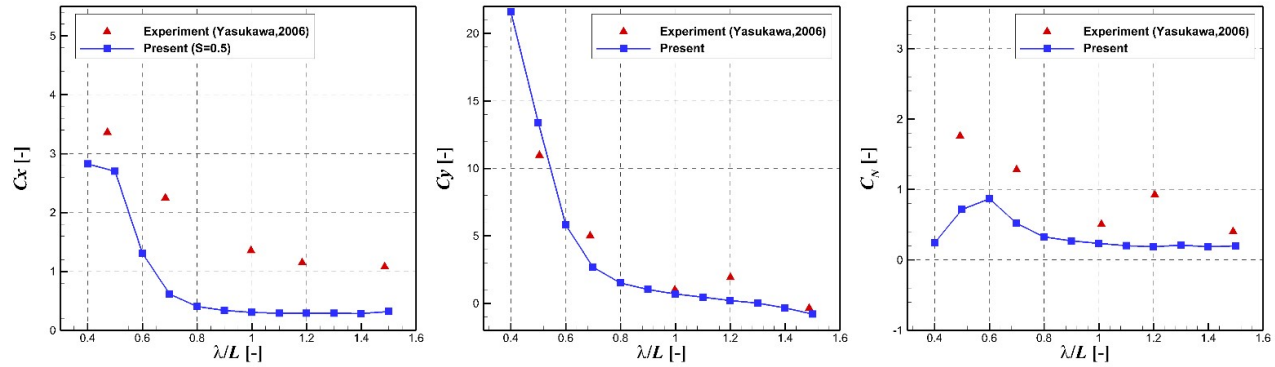

Figure 5: The steady drift forces and yaw moment for the S-175 container ship straightly advancing in regular beam waves

We can see from Fig.5 that the predicted steady sway force agrees well with the experimental data. The predicted surge forces and yaw moment show similar trends with those of the experimental measurements. However, the amplitudes of the numerical results are smaller than the measured values. The discrepancies was related to two reasons. Firstly, there were some numerical errors in the predictions of the first order motions, which corresponding decrease the accuracy of the second order wave forces and moment predictions. Secondly, the flow nonlinearities were caused by, for example, wave breaking or vortex generation, at the ship's ends when the ship is subject to beam waves. These nonlinearities were not captured by the present method, which prevent an accurate resolve of the flow field around the ends of the ship. Considering that the steady surge force is sensitive to the pressure integration at the ship bow and stern, and that distances from the origin of the coordinate to the bow and stern are long, inaccurate solutions of the flow field at the ship's ends could have had a significant effect on the predicted steady surge force and yaw moment. For a better prediction of the steady surge force and yaw moment, taking into account the nonlinearity of the flow is necessary.

After investigating the wave induced motions and the wave drift forces for the straightly advancing ship, we conducted numerical simulations for S-175 container ship obliquely moving in beam waves. Different drift angles namely β=-10°, -5°, 5° were tested in the computations. Note here a minus drift angle indicate that the ship has a transverse speed which opposite to the wave propagation.

Figure 6 computed the steady surge force, the steady sway force and steady yaw moment against the wave length. As we can see, different drift angle lead to different prediction of the steady drift forces, especially in shorter waves. The predicted steady yaw moments under different drift angles show also clear discrepancy.

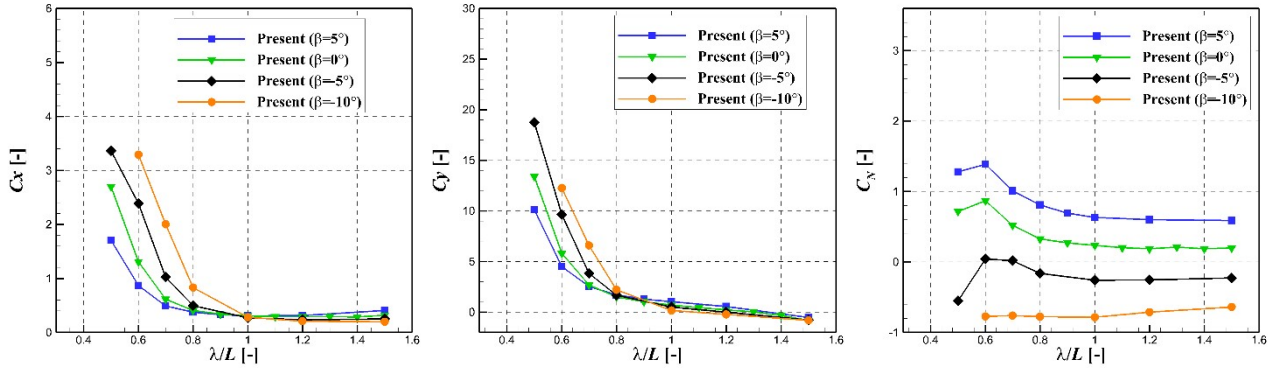

Figure 6: The computed steady drift forces and yaw moment for the S-175 container ship obliquely moving in regular beam waves (plotted against the wave length)

Figs. 7-9 plots the steady surge force, sway force and yaw moment at the wavelengths λ/L=0.5,0.7,1.0. The numerical results are plotted against the drift angle of the hull. Comparative experimental data of Yasukawa and Adnan[14] are also included in the figures.

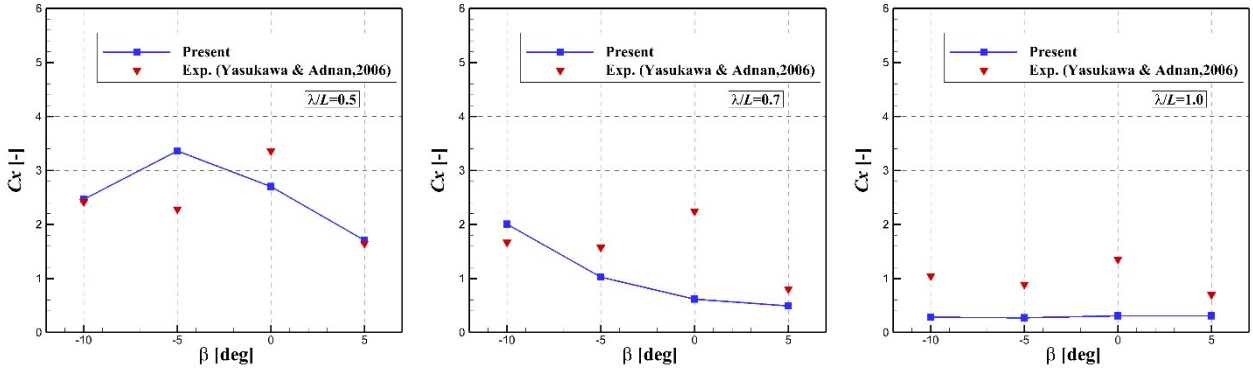

Figure 7: The steady surge force on S-175 container ship obliquely moving in beam waves

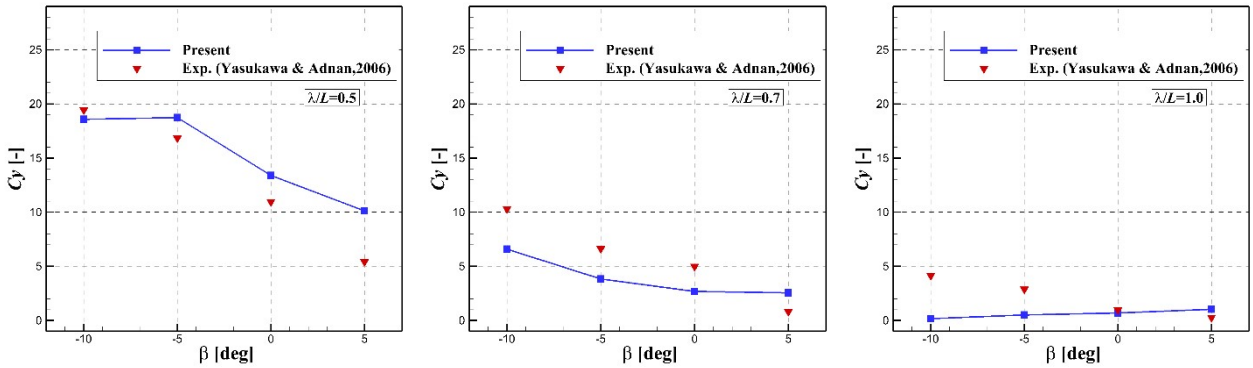

Figure 8: The steady sway force on S-175 container ship obliquely moving in beam waves

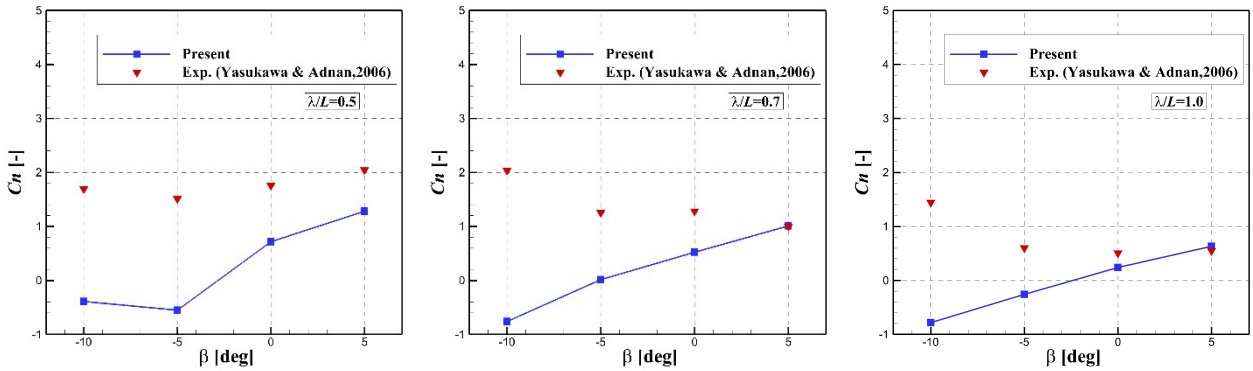

Figure 9: The steady yaw moment on S-175 container ship obliquely moving in beam waves.

We can see from Fig.7 that the numerical results of the steady surge force are generally lower than the experimental data. This may be due to the neglecting of the nonlinearity of the flow in our numerical simulations. However, the related errors were of relatively minor concern because the steady surge force in beam waves were relatively small.

Fig.8 illustrates the comparisons between the computed and measured steady sway forces under different drift angles. We found that the steady sway force acting on the ship with a minus drift angle were obviously higher than those on the straightly advancing ship. Particularly at λ/L=0.5,0.7, the steady sway forces on the ship at β=-10° almost doubled when compared to the values on the ship at β=0. As seen, present results captured the variation trends of those from the experimental measurements. Although there are some discrepancies, the overall agreement between our predictions and the experimentally measured data of Yasukawa and Adnan[14] is satisfactory.

Fig.9 plots the comparisons between the computed and measured steady yaw moment. We can see that present results show different trends as those from the experimental data. The reason for the discrepancy may come from the fact that the steady yaw motion, which was included in the experiments, was not considered in our computations. For a better prediction of the steady yaw moment, more studies are still needed in future.

5 CONCLUSION

A computer code was developed to predict the steady wave drift forces and yaw moment for the obliquely moving ships. The boundary value problem of the classical seakeeping was extended to describe the flow filed around the ship moving with a drift angle. The extended boundary value problem was solved via a time domain Rankine panel method, while the second order wave forces and moments are computed by using a near field pressure integration. The computed mean values of second-order longitudinal, transverse forces and yaw moment represented the steady surge force, the steady sway force, and the steady yaw moment, respectively.

Numerical tests were carried out for the straightly advancing S-175 container ship to validate the developed code. We considered the ship in head and beam waves and compared our numerical results to published experimental measurements. The generally favorable agreement between the present results and the comparative data demonstrated that, although there was some room for improvement, the computational accuracy of our developed method was acceptable form a practical perspective.

By computing the steady wave drift forces and yaw moment acting on an obliquely moving ship, we found the steady sway force are sensitive to the drift angle of the hull. A transverse speed of the ship which opposite to the wave propagation led to obviously increasing of the steady sway force acting on the ship. For a ship moving with a small drift angle, present method could make reasonable prediction of the steady wave drift forces.

ACKNOWLEDGEMENTS

This study was supported by the National Natural Science Foundation of China (Grant no. 51809278) and the Fundamental Research Funds for the Central Universities of China (Grant No. 17CX02012A), to which the first author is most grateful.

REFERENCES

[1] Skejic, R. and Faltinsen, O.M. “A unified seakeeping and maneuvering analysis of ships in regular waves”. In: *Journal of Marine Science and Technology*, 2008,13(4):371-394.

[2] Yasukawa, H. and Nakayama, Y. “6-DOF motion simulations of a turning ship in regular waves”. In: *International Conference on Marine Simulation and Ship Manoeuvrability (MARSIM 2009)*, Panama City, Panama, 2009.

[3] Seo, M.G. and Kim, Y., “Numerical analysis on ship maneuvering coupled with ship motion in waves”. In: *Ocean engineering*, 2011, 38(17-18):1934-1945.

[4] Joncquez, S.A.G. *Second-order forces and moments acting on ships in waves*. Doctoral dissertation, Technical University of Denmark, Copenhagen, Denmark, 2009.

[5] Kim, K. H. and Kim Y. “Numerical study on added resistance of ships by using a time-domain Rankine panel method”. In: *Ocean Engineering*, 2011, 38(13): 1357-1367

[6] Söding, H., Shigunov, V., Schellin, T.E. et al. “A Rankine Panel Method for Added Resistance of Ships in Waves.” In: *ASME J. Offshore Mechanics & Arctic Engineering,,* 136, 031601 (2014), DOI: 10.1115/1.4026847.

[7] El Moctar, O., Sigmund, S., Ley, J., and Schellin, T.E., 2017. “Numerical and experimental analysis of added resistance of ships in waves”. In: *ASME J. Offshore Mechanics & Arctic Engineering, 2017,* 139(1), DOI: 10.1115/1.4034205.

[8] Sigmund, S. and el Moctar, O. “Numerical and experimental investigation of added resistance of different ship types in short and long waves”. In: *Ocean Engineering*, 2018, 147:51-67.

[9] Naito, S., Mizoguchi, S. and Kagawa, K. “Steady forces acting on ships with advance velocity in oblique waves”. In: *Journal of the Kansai Society of Naval Architects*, 1991, 213:45–50.

[10] Ueno, M., Nimura, T., Miyazaki, H., Nonaka, K. “Steady wave forces and moment acting on ships in manoeuvring motion in short waves”. In: *Journal of the Society of Naval Architects of Japan,* 2000, 188:163–172.

[11] Sprenger, F., Maron, A., Delefortrie, G., Van Zwijnsvoorde, T., Cura-Hochbaum, A., Lengwinat, A. and Papanikolaou, A., “Experimental Studies on Seakeeping and Manoeuvrability in Adverse Conditions”, In: *Journal of Ship Research*, 2017. DOI: 10.5957/JOSR.170002.

[12] Wicaksono, A. and Kashiwagi M, “Wave-induced steady forces and yaw moment of a ship advancing in oblique waves”. In *Journal of Marine Science and Technology*, 2017, https://doi.org/10.1007/s00773-017-0510-6.

[13] Yasukawa, H., Hirata, N., Matsumoto, A., Kuroiwa, R. and Mizokami, S. “Evaluations of wave-induced steady forces and turning motion of a full hull ship in waves”. In: *Journal of Marine Science and Technology*, 2018, https://doi.org/10.1007/s00773-018-0537-3.

[14] Yasukawa, H. and Adnan, F.A. “Experimental study on wave-induced motions and steady drift forces of an obliquely moving ship”. In: *Journal of Japan Society of Naval Architects and Ocean Engineers*, 2006, 3:133-138.

[15] Newman, J.N. “The theory of ship motions”. In: *Advances in Applied Mechanics*, 18 (1979): 221-283.

[16] Wu, G.X. “A numerical scheme for calculating the m_j terms in wave-current-body interaction problem”. In: *Applied Ocean Research*. 1991,13(6): 317-319.

[17] Kring, D.C. *Time domain ship motions by a three-dimensional Rankine panel method*, Doctoral dissertation, Massachusetts Institute of Technology, Cambridge, MA, USA. 1994

[18] Zhang, W. and el Moctar, “Numerical prediction of wave added resistance using a Rankine Panel method”, In: *Ocean Engineering*, 2019, (178):66-79.

[19] ITTC, *Recommended Procedures and Guidelines- Numerical Estimation of Roll Damping*, 7.5-02-07-04.5, 2011

[20] Huang, Y. *Nonlinear ship motions by a Rankine panel method*, Doctoral dissertation, Massachusetts Institute of Technology, Cambridge, MA, USA, 1998.